DETECTION AND LOCALIZATION OF DISCONNECTIONS IN A LARGE-SCALE STRING OF PHOTOVOLTAICS USING SSTDR

Ayobami S. Edun, Samuel Kingston, Cody LaFlamme, Evan Benoit,
Michael A. Scarpulla, Cynthia M. Furse, Joel B. Harley

***Abstract*— In this paper, we explore the possibility of using spread spectrum time domain reflectometry (SSTDR) for detecting disconnections in a large-scale photovoltaic array. We discuss the importance, role, and trade-offs of SSTDR resolution, frequency, and attenuation in detecting disconnects in the system. Our results show that if the proper system parameters are chosen, disconnections can be detected in a 1 kV system consisting of twenty-six 60-cell photovoltaic panels and located within 1.52 m for the first 22 modules.**

Index Terms*—*Transmission lines, photovoltaics, spread spectrum time domain reflectometry (SSTDR), fault detection, soft faults.

I. Introduction

Photovoltaic (PV) arrays are subject to numerous kinds of faults. These include ground faults [1], line-to-line faults [2], arc faults [3], open circuits [4], short circuits [4], and faults based on the PV materials [5], [6] . These faults reduce the efficiency of the array and can result in more devastating outcomes, such as fire. To detect these faults, protection devices such as ground fault detection and interruption (GFDI), have been developed. Their primary function is to interrupt the flow of current when it is above their ratings. These devices, however, do not localize faults and can fail to detect faults due to blind spots [7], [8]. For example, if a line-to-line fault occurs under low illumination, the current through the affected string of panels will be low and will not be detected by these conventional systems [7]. Smart inverters [9] and rapid shutdown systems [10], [11] have also been introduced as a way to quickly de-energize an array in the case of a fault or fire. These also do not localize the faults. In this paper, we describe a new fault detection and location method for PV systems -- spread spectrum time domain reflectometry (SSTDR). We evaluate the parameters needed for accurately detecting and locating disconnections (open circuits) in commercial PV systems.

Several works have applied reflectometry to detect faults in transmission lines and PV systems [4], [12]. In this approach, an electromagnetic signal is sent through the electrical system. This signal reflects at points of impedance mismatch. After correlating the incident and reflected signal, the time delay gives the distance to the fault, while the amplitude and phase of the reflection give the strength and characteristics of the impedance mismatch [13]. There are several variations of reflectometry [14]. Time domain reflectometry (TDR) uses a short rise time voltage step as the incident voltage while spread spectrum time domain reflectometry (SSTDR) uses a modulated pseudo-noise (PN) code as the test signal. Unlike TDR [15], [16] and other reflectometry methods, SSTDR is robust to noise and can be used on live systems [17].

For several SSTDR analysis methods, baseline subtraction is used to detect faults [18]–[20]. SSTDR transmits a signal into the PV array, and the reflections are measured at the source to analyze the state of the system. The baseline reflection signature of the setup without fault is first obtained and stored. New reflection signatures are then subtracted from the baseline to isolate regions with differences from the baseline, indicating faults or other changes in the system that result in a change to the system impedance. This method has the advantage that it removes the normal reflections from cables and connectors [19].

Even with baseline subtraction, noise and attenuation make fault localization difficult. One algorithm has addressed this by identifying the first location where the reflection signature deviates from the baseline to locate disconnections [19]. In this method, baseline subtraction is performed and then a pre-set threshold is used to determine the first point that deviates from zero. The location of the deviation estimates the location of the disconnection. Empirically, this method works well for a setup with fewer than eight panels. As the number of panels increases, the magnitude of the reflection coefficient of a disconnection becomes weaker than the threshold. As a result, a critical challenge with reflectometry is that signals attenuate quickly as they travel through a PV string, experiencing multiple reflections (each getting smaller), eventually reaching the noise floor. Consequently, prior work that uses reflectometry to detect disconnections in PV strings has been limited to arrays of less than ten panels [19], [21]. This is still far smaller than commercial systems, which are usually comprised of tens of panels. While settings in the SSTDR can be changed to accommodate longer distances (e.g., decreasing modulation frequency), there are trade-offs (e.g., loss of resolution) that need to be well understood. In addition, the parameters of PV panels (e.g., effectively electrical length and attenuation) need to be considered.

This paper studies these trade-offs and describes how to choose key parameters needed for accurately detecting and locating disconnections in commercial PV arrays (26 or more panels that

This paragraph of the first footnote will contain the date on which you submitted your paper for review. It will also contain support information, including sponsor and financial support acknowledgment. For example, “This work was supported in part by the U.S. Department of Commerce under Grant BS123456.”

Ayobami S. Edun, Cody LaFlamme, and Joel B. Harley are with the Department of Electrical and Computer Engineering, University of Florida, Gainesville, FL 32611 USA (e-mail: aedun@ufl.edu; flyingcod-fish@ufl.edu; joel.harley@ufl.edu).

Samuel R. Kingston, Evan J. Benoit, and Michael Scarpulla are with the Department of Electrical and Computer Engineering, The University of Utah, Salt Lake City, UT84112. USA (e-mail: samuel.kingston@utah.edu; evan.benoit@utah.edu; mike.scarpulla@utah.edu).

Cynthia M. Furse is with the Department of Electrical and Computer Engineering, The University of Utah, Salt Lake City, UT 84112 USA, and with LiveWire Innovation, Camarillo, CA 93012 USA (e-mail: cfurse@ece.utah.edu)

carry 1 kV or more). A 1-kV string was considered because this is the maximum rating of our SSTDR device.

We describe the important factors (resolution, attenuation, and travel distance) that need to be considered when conducting experiments with SSTDR. We also discuss how to interpret the SSTDR signatures. To validate our approach, we perform SSTDR experiments with an array of twenty-six (26) 60-cell, 40.81V, industry-sized panels. These are configured symmetrically with the same number of panels on either side of the transmission line as in Fig. 1. Our results show that we can detect disconnections within a string of 26 panels rated up to 1 kV with location accuracy within one module.

The rest of this article is organized as follows. In Section II, we give a background on SSTDR, a description of our experimental setup, and an explanation of the role of panel length, system modulation frequency, and attenuation on SSTDR signals. In section III, we discuss the results of the choice of system parameters in locating disconnects in our setup. Finally, in section IV, we give our conclusions and future work.

II. SSTDR Experimental Design

Detecting faults in a string of tens of panels is more complex than a few panels due to multiple reflections and attenuation. Also, the size of the panel, the length of the leader cable, and the modulation frequency of the input signal all affect our data. This section studies what signal or panel parameters affect the SSTDR data and how they influence the ability to detect disconnections in a PV array. We discuss the effects of four specific design parameters in our SSTDR experiments: (1) the modulation frequency and its effect on spatial resolution, (2) the electrical length of a PV panel, (3) the modulation frequency and its effect on attenuation, and (4) the number of panels and their effect on attenuation.

A. SSTDR Background

SSTDR is based on the reflection of an incident signal through a transmission line. SSTDR transmits a spread spectrum signal into a transmission line and then measures and analyzes the reflections received at the sending end of the line. The incident SSTDR signal is a PN code modulated by a square (or sine) wave. The pseudo-random sequence has statistical characteristics similar to Gaussian noise [22]. The incident wave sent down a transmission line is reflected at every point of impedance discontinuity [23]. The reflected signal is then correlated with a delayed version of the incident signal to produce the reflectometry signature to be analyzed. To calculate the distance to a fault, the time-domain axis is multiplied by the velocity of propagation to show the signal as a function of distance [24].

When the end of the line is an open circuit, we expect a perfect reflection with a reflection coefficient (the ratio of reflected to transmitted voltage) of 1. Similarly, a short circuit gives a reflection coefficient of -1 [25]. More generally, negative reflection coefficients represent loads with an impedance less than the transmission line characteristic impedance, while positive reflection coefficients signify a load with higher impedances than the transmission line characteristic impedance.

Table 1: PV Panel Characteristics

PV Panel Characteristics [12]	
Module Manufacturer	Piemar
Module Type	SG310M(FB)
Max power at STC (Pmax)	310W
Open Circuit Voltage (Voc)	40.81V
Optimum operating current (Imp)	9.27A
Optimum operating voltage (Vmp)	33.45
Max. system voltage	1500V
Short circuit current (Isc)	9.92A
Max. series fuse rating	15A

B. Experimental Setup

For our experiments, we used 60-cell PV modules manufactured by Piemar [26]. The characteristics of the panels are shown in Table 1. The panels were located at Gardner Energy in West Haven, Utah. The SSTDR box was connected to 26 Piemar PV panels in series, as shown in Fig. 1. In this setup, we connected a 15.24 m (50 ft) twin-lead leader cable with parameters given in [19] from the SSTDR to the panels using an MC4 connector. Panels are connected using MC4 connectors in a symmetric arrangement (the same number of panels located on the positive and negative sides of the transmission line). The length of the cable connecting each panel is about 2.13 m (7 feet). Each panel connection is labeled in Fig. 1.

We perform three experimental studies (described in the following subsections). The first experiment is used to determine the equivalent electrical length of a single PV panel. The second experiment studies how the SSTDR reflection signature changes with the modulation frequency. The third experiment is aimed at quantifying the number of panels across which the SSTDR signal can travel while still able to detect disconnections.

C. Disconnect Localization Requirements

We tune our SSTDR system to satisfy two requirements. First, the SSTDR must be able to confidently locate faults between any two PV panels. These requirements would allow a maintainer to rapidly identify the cabling that must be inspected or replaced. Second, the SSTDR must be able to monitor the entire PV array. This requirement ensures that no part of the PV array is missed by our system.

These two requirements are balanced by the trade-offs in SSTDR resolution and attenuation. The SSTDR attenuation must be small enough that the SSTDR signal can travel through all 26 panels. The SSTDR resolution must be fine enough so that its maximum value can be reliably found within the distance between two panels. Note that measuring distance is not obvious. While the length of the cables connecting each

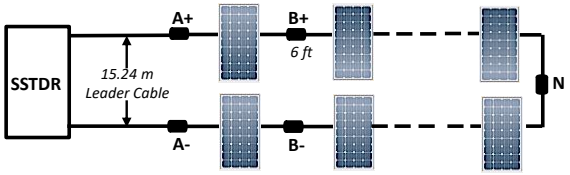

Fig. 1: Setup with a string of 26 panels

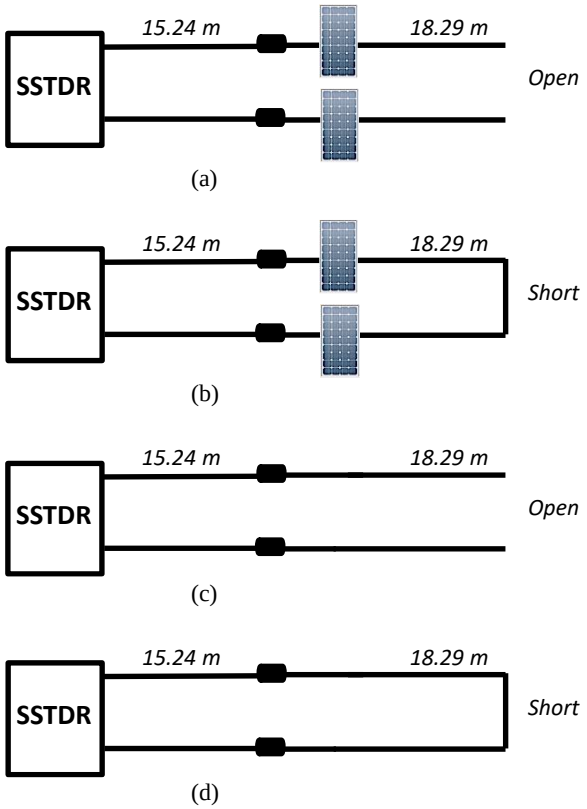

Fig. 3: Experimental setups used to extract both the transmission and reflection coefficients as (a) Panel-Open, (b)Panel-Short, (c) Cable-Open, (d) Cable-Short.

panel is straightforward to measure, the panels themselves have an electrical length that must be accounted for.

To identify the equivalent electrical length of a single panel, we measure SSTDR reflection signatures corresponding to the experimental setups illustrated in Fig. 3. We refer to these setups as (a) panel-open, (b) panel-short, (c) cable-open, and (d) cable-short, respectively. Since the panel has an equivalent electrical length, the location of the reflection from the end of the line should be greater when there is a panel in the line (as in Fig. 3 (a), (b)) compared to when there is no panel in the line (as in Fig. 3 (c), (d)). To measure the equivalent electrical length Δd of the solar panels, we isolate the reflection from the end of the line according to

$$x_{panel}(t) = \frac{x_p^{(open)}(t) - x_p^{(short)}(t)}{2} \quad (1)$$

$$x_{cable}(t) = \frac{x_c^{(open)}(t) - x_c^{(short)}(t)}{2} \quad (2)$$

where $x_p^{(open)}(t)$, $x_p^{(short)}(t)$, $x_c^{(open)}(t)$, and $x_c^{(short)}(t)$ are the panel-open, panel-short, cable-open, and cable-short time-domain SSTDR measurement from Fig. 3, respectively.

The new time-domain SSTDR reflection signatures $x_{panel}(t)$ (dashed line in red) and $x_{cable}(t)$ (solid line in blue) are shown in Fig. 2. Note that both lines retain reflections only from the end of the cable. This is because the subtracted signals ($x_p^{(open)}(t)$ and $x_p^{(short)}$, $x_c^{(open)}(t)$ and $x_c^{(short)}(t)$) are

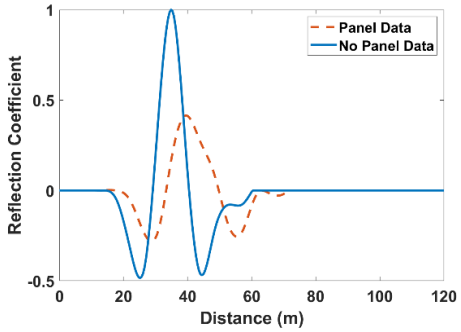

Fig. 2: SSTDR data for in-line panels (dashed) and no panels (solid) with a modulation frequency of 6 MHz.

equivalent except that except that the reflection from the end of the cable has a reversed polarity of the other.

The data was then analyzed in the frequency domain by computing the magnitude and phase response of the data. It is expected that the length of the panel should be captured in the phase delay of $x_{panel}(t)$ (panel data) with respect to $x_{cable}(t)$ (no panel data). Using the no-panel data ($x_{cable}(t)$) as a reference, we note the frequency with the highest energy (say f_e) and calculate the delay between both signatures $x_{panel}(t)$ and $x_{cable}(t)$ at this frequency (f_e). The effective distance Δd through the panel is then estimated by multiplying the obtained phase delay by the velocity of propagation ($v = 0.721c$), where c is the vacuum phase velocity of EM waves or light. The time delay Δt_f is calculated as

$$\Delta t_f = \left(\frac{\Delta\phi}{360}\right) T \quad (3)$$

where $\Delta\phi$ is the phase delay at the appropriate frequency f_e, and T is the period at the same frequency f_e.

The frequency with the highest energy value for $x_{cable}(t)$ is 4.22 MHz and is labeled on the top subplot of Fig. 4. The associated phase values for both $x_{cable}(t)$ and $x_{panel}(t)$ are 6.88 degrees and -82.0 degrees, respectively, and are labeled on the lower subplot of Fig. 4. Thus, the phase shift $\Delta\phi$ = 6.88 – (-82.0) = 88.9 degrees, and the period $T = \frac{1}{4.22MHz} = 237\ ns$. According to (3), for time delay Δt_f = 58.5 ns, the distance is calculated as:

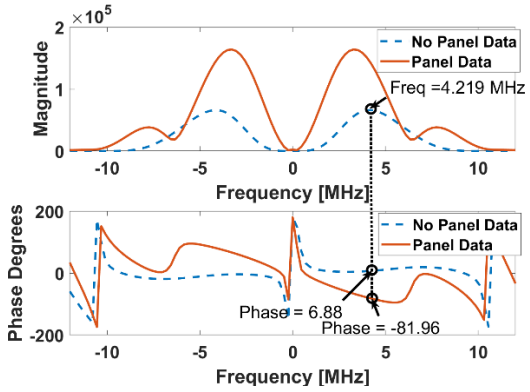

Fig. 4 : Frequency and phase of the panel data, $\theta(t)$ and no panel data, $\theta(t)$. The frequency, f_e that corresponds to the maximum energy is also shown with its corresponding phase.

$$\Delta d = \left(\frac{1}{2}\right) v \Delta t_f = 6.32m \quad (4)$$

where the division by 2 accounts for round trip time. The distance $6.32\,m$ (20.73 ft) is the estimated effective distance through the panel and its connecting cables. Each connecting cable on both sides of the panel is 1.07 m (3.5 ft) long, so the panel itself is estimated to have an electrical length of about 6.32 – 2(1.07) = 4.18 m.

Note that the electrical panel length can differ based on panel type and manufacturer, but the process described in this paper can be used for all types of panel.

D. Determining SSTDR Resolution

Existing SSTDR hardware comes with different modulation frequencies, ranging from 93.75 kHz to 48.0 MHz, depending on the device type. The device, which is available commercially [27], can come with either a WILMA board [27] or Arnold [28]. The WILMA board has a maximum modulation frequency of 48 MHz while the Arnold board has 24 MHz as the maximum. Hence, the WILMA board gives ten reflection signatures, one for each of the ten modulation frequencies it supports, with the lowest being 93.75 kHz. The next frequency is twice the previous until the maximum of 48 MHz. The Arnold board gives nine reflection signatures with a maximum of 24 MHz as the center or modulation frequency.

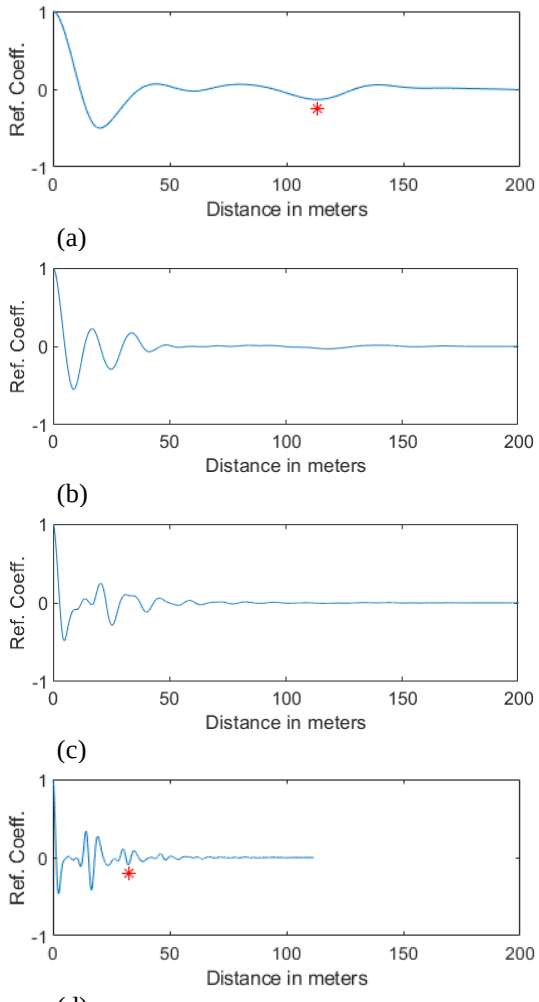

Fig. 5: a) Reflection signature with modulation frequency SSTDR signal of a) 3MHz. b) 6MHz. c) 12MHz. d) 24MHz for the setup in Fig. 1

Fig. 5 shows the SSTDR reflection signature of the system for four different frequencies. As the signal propagates through the experimental system, it is reflected at every panel, which represents an impedance change. As the modulation frequency increases, the pulse width of the signal decreases, and more reflections are distinctly visible in the signal. The resolution of the SSTDR signal can be defined by the half-amplitude width of the time-domain signal, as illustrated in [24]. For an SSTDR system, the time-width of the signal main lobe in meters is:

$$\sigma_w = \frac{v}{3\,f_c} \quad (5)$$

where f_c is the system's modulation frequency, and v is the velocity of propagation. As the modulation frequency increases, SSTDR achieves more precise detection and localization. This means we can detect more closely spaced faults using higher frequencies. In addition, knowing the precision allows us to confidently identify the faults within a region of the PV array.

Based on (5), SSTDR frequencies of 24 MHz, 12 MHz, and 6 MHz have resolutions of 3 m (or $\pm$1.5 m), 6 m (or $\pm$ 3 m), and 12 m (or $\pm$6 m), respectively. Given the requirements to locate the maximum within a 6.32 m region, the length of a panel, and its connecting cables, frequencies lower than 5.7 MHz cannot reliably locate faults between two panels due to poor resolution. The minimum frequency required for this setup to have a good resolution is 5.7 MHz. In general, the minimum frequency required to have a good resolution for fault detection can be estimated using equation (5) where d_w is twice the length of the panel and its connecting cables (2 × 6.32 m in our case) and not just the length of the panel alone. While 24 MHz may initially appear the best option due to its improved precision, higher frequencies are more affected by attenuation. We study this effect in the next subsection.

E. Using 24 MHz SSTDR modulation frequency

We conduct a third experiment for the same setup in Fig. 1 with 26 panels connected in series. We first obtain a baseline reflection signature using 24 MHz modulation frequency, then we introduce disconnections at A+, A-, B+, B-, C+, …, N. We then subtract the reflection signature of each disconnection from the baseline. Fig. 6 shows the 24 MHz baseline subtracted signals for the setup in Fig. 1. We split the figure into two for better analysis and clarity. Fig. 6(a) shows the baseline subtracted signals for disconnects at A- to D- while Fig. 6(b) shows the baseline subtracted signals for disconnects at H- to N. Since our setup is symmetric, we expect to get the same reflection signature from the positive and negative side of the wire. That is, the reflection signature of the disconnects at A+ should be the same as at A-, as in [25].

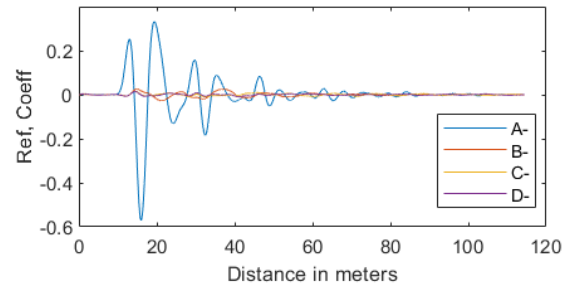

(a)

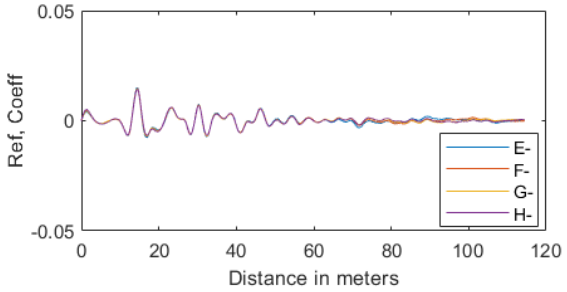

(b)

Fig. 6: (a) Baseline subtracted signals for locating disconnects using 24 MHz modulation frequency in locations A to D (b) E to H.

Observe in Fig. 6(a) that the reflection signature of each disconnection can be distinguished. As we move down the array, the magnitude of the baseline subtracted reflection signature reduces significantly and stops changing thereby yielding overlapping signatures, as illustrated in Fig. 6 (b). This is because there is a high attenuation (as explained in the next subsection) at this frequency, regardless of resolution. Consequently, the baseline subtraction at 24 MHz gives us good precision and can help detect and locate faults up to 4 panels in a symmetric configuration if the peaks of the signals are used to locate faults. An example of good precision in the localization of faults is the peak of the reflection at A-, where we can see that the peak is sharp and can be easily distinguished. To locate disconnections in a greater number of panels, we need to go to lower frequencies.

F. Determining SSTDR Attenuation

To estimate the role of attenuation in detecting disconnects in a photovoltaic array, we compare the baseline subtracted signals for 6 MHz, 12 MHz, and 24 MHz. We explore how attenuation varies with both the number of panels and the SSTDR modulation frequency. While higher frequencies improve precision, the distance the signal can propagate decreases. This is because higher frequencies attenuate faster than lower frequencies. For example, Fig. 5 shows that the 24 MHz frequency has approximately the same magnitude after traveling 30.48 m as the 3 MHz frequency has after traveling 106.68 m as shown with the '*' marker in Fig. 5. In addition, as we add panels to the array, the energy of the signal will get reduced from reflecting between panels and will not be measured at the SSTDR. Hence, the number of panels play a large role in attenuation in the system.

To study the attenuation as a function of frequency, we compute the analytic signal (taking the Hilbert transform) of all SSTDR baseline subtracted reflection signatures as shown in Fig. 7 for

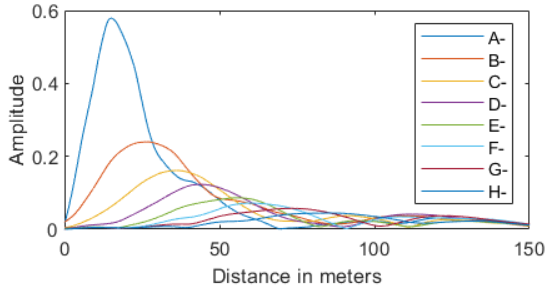

Fig. 7: Plot of envelope (analytic) signal (*with a modulation frequency of 6 MHz*) for the baseline subtracted reflection signature corresponding disconnection location A to H.

disconnection at A to H using 6 MHz modulated input signal. We repeat this for each SSTDR frequency. For each set of disconnection data, we compute the L_2 *norm* of the data (i.e., the square root of the signal's sum of square). The L_2 *norm* metric is chosen instead of the maximum of each analytic signal because as we add more panels, the location of the maximum value quickly becomes indistinguishable for frequencies above 6 MHz (12 MHz and 24 MHz, in this case). Also, since the reflection coefficient is less than 1, the sum of squares of values less than 1 quickly goes to 0. Hence, using the norm (square root of energy) is better than using the energy itself.

We then measure the relative drop in the baseline subtracted SSTDR signal's L_2 *norm* (or norm) as a function of disconnection location. Fig. 8 illustrates how this metric drops for our three chosen frequencies. We observe that the 24 MHz signal loses 95% of its norm after 4 panels and the 12 MHz signal loses 95% of its norm after 8 panels. Hence, halving the frequency from 24MHz results in approximately doubling the number of panels the signal can go through before losing 95% of its norm. This analysis suggests that for SSTDR frequency f_p, we can define the number of panels N_p before an input signal loses 95% of its norm according to

$$N_p = \frac{96 \times 10^6}{f_p} \tag{6}$$

.

To identify the frequency capable of detecting faults with N_p number of panels, we can solve for f_p using equation (6).

Fig. 9 shows the number of panels against frequency and the SSTDR resolution in meters against frequency. The red star

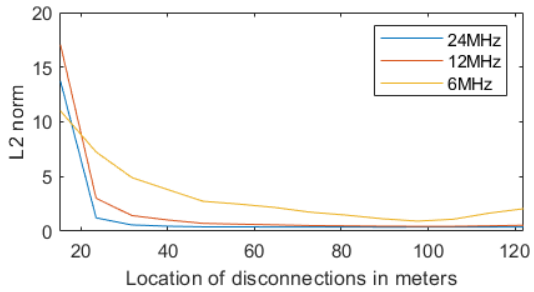

Fig. 8: L2 norm of the envelope of each baseline subtracted SSTDR signal from disconnections for modulation frequencies 24MHz, 12MHz and 6 MHz as a function of location of the disconnection.

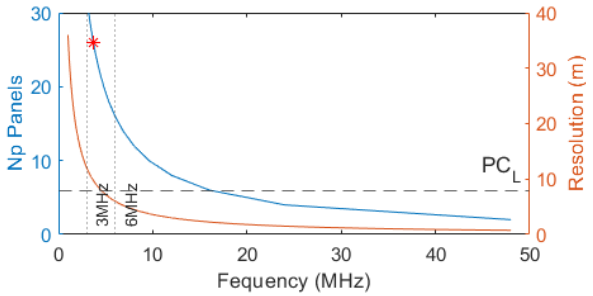

Fig. 9: Frequency required for Np panels and the corresponding resolution of each frequency.

marker shows that for 26 panels, a frequency of 3.69 MHz is appropriate. However, the resolution of the SSTDR signal, (as defined in (5)) at this frequency is higher than the panel length. Recall that the resolution (half-width of the SSTDR pulse) must be lower than the panel electrical length for a fault to be detected between two panels. Hence, SSDTR signal at 3.69 MHz cannot be used to detect faults in this setup. Fig. 9 shows that the minimum frequency that meets the resolution requirement is about 5.7 MHz. Also, note that 6 MHz retains at least 95% of its norm for most of the length of the PV array (approx. 121.92 m). For these reasons, we focus on the next available SSTDR frequency after 5.7 MHz, which is 6 MHz.

To then study attenuation of the 6 MHz SSTDR signal as a function of the number of panels, we observed the reduction in the maximum value of the analytic signal in Fig. 7. The analytic signal of each baseline subtracted reflection signatures is the signal plus its Hilbert transform. Fig. 10 shows these maximum values as a function of distance (which corresponds to a distance in the array) at the 6 MHz modulation frequency. We fit this curve to a power law function defined by:

$$g(d) = b\left(\frac{1}{d}\right)^{c} \quad (7)$$

where d is the distance traveled in the system setup, and b and c are constants that control the fit. The coefficients of our fit, which are learnt from the data, are b = 31.6 (28.7, 34.6) and c = 1.48 (1.44, 1.51), where the values in parenthesis show a 95% confidence interval. Using this model, we can estimate the maximum amplitude of the SSTDR reflection signature and, subsequently, the number of panels we can theoretically see through.

Based on previous measurements, albeit on a different PV system, the noise floor of SSTDR measurements is about 0.005 for variation within individual PV panels as explained in [29]. Equation (7) reveals the maximum distance we can see through for this noise floor is 366 m. So, with our experimental setup, a leader cable of 15.24 m, a panel plus cable length, PC_L of 6.32 m, it implies that at 6 MHz, we can theoretically detect disconnects in a setup that contains up to 58 panels. This is because, although about 95% of the signal has been lost after going through the panels in our setup, the signal is still above the noise floor of the system. More details about localization are included in the next section.

In conclusion, this section demonstrates that the available 6 MHz SSTDR modulation frequency is the best to satisfy our two requirements. First, it can confidently identify faults between two panels. Second, it can interrogate each of the 26 panels in the PV array. We demonstrate the capabilities of the 6 MHz to locating disconnections in the next section.

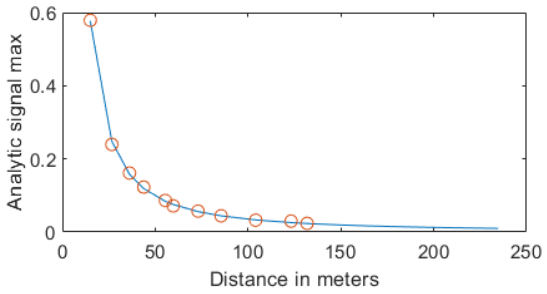

Fig. 10: Plot of maximum of each analytic signal against distance in meters and fitting an exponential to estimate attenuation.

III. LOCATING DISCONNECTIONS

In [6], the point of deviation between the reflection signature and baseline was used to localize faults. In our case, we will use the peak of the signals to detect and locate the faults since we do not have overlapping reflection signatures.

A. Using 6 MHz SSTDR modulation frequency

Fig. 11 shows the baseline subtraction results for the 6 MHz modulation frequency. Observe that the peaks of each baseline subtracted reflection signature are distinct and can be used to locate the distance of each disconnection from the SSTDR. To quantify the disconnection locations, we record the peaks of each baseline subtracted signal. The locations of these peaks are denoted as "SSTDR estimated" are shown in the second column of Table 2. The third column denoted as "Location in string" is the actual measured distance of the connector in the

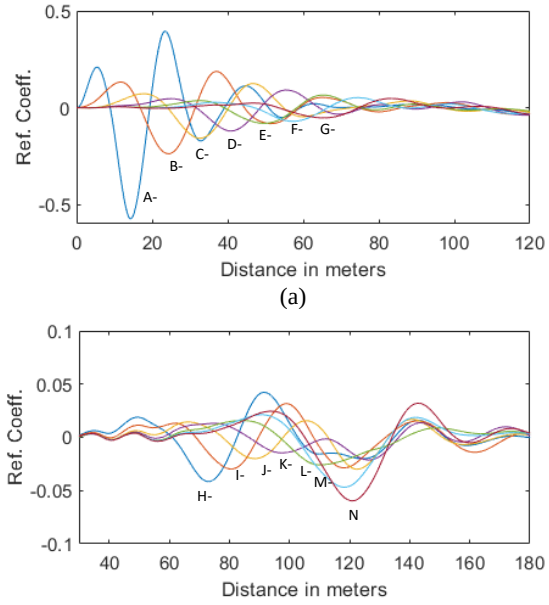

Fig. 11: Baseline subtracted signals for locating disconnections using 6 MHz modulation frequency in locations (a) A to G (b) H to N.

Table 2: Estimated and effective locations of disconnect across experimental system.

Breaks	SSTDR Estimated (m)	Location in String (m)	Corrected Location (m)	Error (m)
A-	14.34	15.24	15.24	0.90
B-	24.37	17.07	23.47	0.90
C-	32.74	18.90	31.70	1.04
D-	40.97	20.73	39.93	1.04
E-	49.77	22.56	48.16	1.61
F-	57.45	24.38	56.39	1.06
G-	65.62	26.21	64.62	1.00
H-	73.24	28.04	72.85	0.39
I-	80.95	29.87	81.08	0.13
J-	88.64	31.70	89.31	0.67
K-	97.63	33.53	97.54	0.09
L-	110.40	35.36	105.77	4.63
M-	118.54	37.19	114.00	4.54
N	121.24	39.01	122.23	0.99

experimental setup. All values in the table are raw values in meters. Observe that the difference between the actual disconnect location (third column) and the peak of the estimated location of the disconnection (second column) is large. This affirms our earlier conjecture (as discussed in section C) that each panel has an effective electrical length (P_L), but it was not accounted for in the third column of Table 2. Although the prior experiment (in Section C) suggests a P_L of 4.18 m, correcting the disconnection location with 4.18 m still gave a high error. Based on observation of the data, we found that correcting with a length of 6.32 m (PC_L), instead of 4.18 m (P_L), to be more appropriate in correcting the disconnection location. This disparity is probably due to some velocity of propagation change within the panel when there is more than one panel.

We add $6.32n$ to each disconnection location (column 3), where n is the number of panels before that location. The corrected disconnect locations are shown in the 4th column of Table 2, denoted as "Corrected Location". By doing this, the error in the location accuracy of the disconnections was reduced significantly. Specifically, we can locate faults within one panel (including its connecting cables, the electrical length is 6.32 m) for all locations. For the disconnects at L- and M-, we observed some overlaps in the multiple reflections which caused a larger error. However, the disconnect can still be located within the length of one panel. Summarily, we were able to locate disconnections in a string of 26 panels rated 1 kV to within one panel using a 6 MHz SSTDR signal.

IV. CONCLUSIONS AND FUTURE WORK

The viability of spread spectrum time domain reflectometry to detect disconnections and other kinds of faults in an experimental setup of fewer than ten panels has been shown in various works. To further strengthen the applicability of SSTDR, this work has extended prior works to explore the possibility of detecting and locating faults in a PV array with 26 panels, rated 1 kV.

The trade-offs that exist between attenuation and resolution in detecting disconnections were explored in this paper. The role of the electrical length of a PV panel has also been explored. While 24 MHz initially appeared to be the best frequency to use, due to its high resolution, it is highly attenuated and therefore cannot probe large arrays. Lower frequencies have a low resolution, but their lower attenuation can make them a better choice for locating disconnections in these systems. For our setup, the frequency of 3.69 MHz enabled sufficient power to reach the panels but did not provide sufficient resolution. A frequency of at least 5.7 MHz was needed for the resolution. Based on these constraints, a 6 MHz SSTDR frequency was chosen. This allowed detection and location of disconnections in a 1 kV photovoltaic system of 26 panels. This work has also provided a theoretical estimation of how far (distance or number of panels) from the SSTDR a disconnection can be detected and located. Our work can be used by fleet owners to detect disconnects in a 1 kV setup. Arc faults, ground faults, and other kinds of faults in similar large-scale setup will be considered in a future work.

Acknowledgment

This material is based upon work supported by the U.S. Department of Energy's Office of Energy Efficiency and Renewable Energy (EERE) under Solar Energy Technologies Office (SETO) Agreement Number DE-EE0008169. Thanks to Gardner Energy (West Haven, UT) for their support in conducting testing on their PV modules.

References

[1] M. K. Alam, F. Khan, J. Johnson, and J. Flicker, "A Comprehensive Review of Catastrophic Faults in PV Arrays: Types, Detection, and Mitigation Techniques," *IEEE Journal of Photovoltaics*, vol. 5, no. 3, pp. 982–997, May 2015, doi: 10.1109/JPHOTOV.2015.2397599.

[2] D. S. Pillai, F. Blaabjerg, and N. Rajasekar, "A Comparative Evaluation of Advanced Fault Detection Approaches for PV Systems," *IEEE Journal of Photovoltaics*, vol. 9, no. 2, pp. 513–527, Mar. 2019, doi: 10.1109/JPHOTOV.2019.2892189.

[3] W. Fenz, S. Thumfart, R. Yatchak, H. Roitner, and B. Hofer, "Detection of Arc Faults in PV Systems Using Compressed Sensing," *IEEE Journal of Photovoltaics*, vol. 10, no. 2, pp. 676–684, Mar. 2020, doi: 10.1109/JPHOTOV.2020.2965397.

[4] M. U. Saleh *et al.*, "An Overview of Spread Spectrum Time Domain Reflectometry Responses to Photovoltaic Faults," *IEEE Journal of Photovoltaics*, vol. 10, no. 3, pp. 844–851, May 2020, doi: 10.1109/JPHOTOV.2020.2972356.

[5] A. J. Beinert, P. Romer, M. Heinrich, M. Mittag, J. Aktaa, and D. H. Neuhaus, "The Effect of Cell and Module Dimensions on Thermomechanical Stress in PV Modules," *IEEE Journal of Photovoltaics*, vol. 10, no. 1, pp. 70–77, Jan. 2020, doi: 10.1109/JPHOTOV.2019.2949875.

[6] N. Bosco, T. J. Silverman, and S. Kurtz, "The Influence of PV Module Materials and Design on Solder Joint Thermal Fatigue Durability," *IEEE Journal of Photovoltaics*, vol. 6, no. 6, pp. 1407–1412, Nov. 2016, doi: 10.1109/JPHOTOV.2016.2598255.

[7] Z. Li, Y. Yu, C. Wu, Z. Yang, and J. Meng, "Detection of High-Impedance Line-Line Fault in Photovoltaic

Arrays Based on Voltage Divider," in *2019 IEEE Sustainable Power and Energy Conference (iSPEC)*, Nov. 2019, pp. 786–791, doi: 10.1109/iSPEC48194.2019.8975269.

[8] J. Flicker and J. Johnson, "Photovoltaic ground fault and blind spot electrical simulations.," SAND2013-3459, 1089985, Jun. 2013. doi: 10.2172/1089985.

[9] D. Montenegro and M. Bello, "Coordinating Control Devices and Smart Inverter Functionalities in the Presence of Variable Weather Conditions," in *2018 IEEE/PES Transmission and Distribution Conference and Exposition (T D)*, Apr. 2018, pp. 1–9, doi: 10.1109/TDC.2018.8440465.

[10] W. Bower, "National electrical code changes in 2014 for photovoltaics: Processes, critical industry consensus topics and impacts," in *2014 IEEE 40th Photovoltaic Specialist Conference (PVSC)*, Jun. 2014, pp. 3352–3355, doi: 10.1109/PVSC.2014.6925653.

[11] A. Cordova, C. Merz, G. Bettenwort, M. Hopf, H. Knopf, and J. Laschinski, "Rapid Shutdown with Panel Level Electronics-A suitable safety measure?," in *2017 IEEE 44th Photovoltaic Specialist Conference (PVSC)*, Jun. 2017, pp. 1965–1967, doi: 10.1109/PVSC.2017.8366726.

[12] C. M. Furse, M. Kafal, R. Razzaghi, and Y.-J. Shin, "Fault Diagnosis for Electrical Systems and Power Networks: A Review," *IEEE Sensors Journal*, 2020.

[13] C. Furse, P. Smith, C. Lo, Y. C. Chung, P. Pendayala, and K. Nagoti, "Spread spectrum sensors for critical fault location on live wire networks," *Structural Control and Health Monitoring*, vol. 12, no. 3–4, pp. 257–267, 2005, doi: 10.1002/stc.69.

[14] C. Furse, Y. C. Chung, C. Lo, and P. Pendayala, "A critical comparison of reflectometry methods for location of wiring faults," 2006, doi: 10.12989/sss.2006.2.1.025.

[15] T. Takashima, J. Yamaguchi, K. Otani, K. Kato, and M. Ishida, "Experimental Studies of Failure Detection Methods in PV Module Strings," in *2006 IEEE 4th World Conference on Photovoltaic Energy Conference*, May 2006, vol. 2, pp. 2227–2230, doi: 10.1109/WCPEC.2006.279952.

[16] T. Takashima, J. Yamaguchi, and M. Ishida, "Fault detection by signal response in PV module strings," in *2008 33rd IEEE Photovoltaic Specialists Conference*, May 2008, pp. 1–5, doi: 10.1109/PVSC.2008.4922843.

[17] P. Smith, C. Furse, and J. Gunther, "Analysis of spread spectrum time domain reflectometry for wire fault location," *IEEE Sensors Journal*, vol. 5, no. 6, pp. 1469–1478, Dec. 2005, doi: 10.1109/JSEN.2005.858964.

[18] S. Roy, M. K. Alam, F. Khan, J. Johnson, and J. Flicker, "An Irradiance-Independent, Robust Ground-Fault Detection Scheme for PV Arrays Based on Spread Spectrum Time-Domain Reflectometry (SSTDR)," *IEEE Transactions on Power Electronics*, vol. 33, no. 8, pp. 7046–7057, Aug. 2018, doi: 10.1109/TPEL.2017.2755592.

[19] M. U. Saleh *et al.*, "Detection and Localization of Disconnections in PV Strings Using Spread-Spectrum Time-Domain Reflectometry," *IEEE Journal of Photovoltaics*, vol. 10, no. 1, pp. 236–242, Jan. 2020, doi: 10.1109/JPHOTOV.2019.2953392.

[20] M. K. Alam, F. H. Khan, J. Johnson, and J. Flicker, "PV arc-fault detection using spread spectrum time domain reflectometry (SSTDR)," in *2014 IEEE Energy Conversion Congress and Exposition (ECCE)*, Sep. 2014, pp. 3294–3300, doi: 10.1109/ECCE.2014.6953848.

[21] N. K. Tumkur Jayakumar, M. U. Saleh, E. Benoit, J. Lacombe, M. Scarpulla, and C. Furse, "Fault Detection In PV Strings Using SSTDR," in *2018 USNC-URSI Radio Science Meeting (Joint with AP-S Symposium)*, Jul. 2018, pp. 9–10, doi: 10.1109/USNC-URSI.2018.8602847.

[22] H. Zhao, C. Xian, Y. Yu, and F. Zhao, "Detection Method of Low Voltage Cable Fault Point Based on SSTDR Technology," in *2019 6th International Conference on Dependable Systems and Their Applications (DSA)*, Jan. 2020, pp. 151–158, doi: 10.1109/DSA.2019.00026.

[23] C. Furse, You Chung Chung, R. Dangol, M. Nielsen, G. Mabey, and R. Woodward, "Frequency-domain reflectometry for on-board testing of aging aircraft wiring," *IEEE Transactions on Electromagnetic Compatibility*, vol. 45, no. 2, pp. 306–315, May 2003, doi: 10.1109/TEMC.2003.811305.

[24] N. K. T. Jayakumar *et al.*, "Postprocessing for Improved Accuracy and Resolution of Spread Spectrum Time-Domain Reflectometry," *IEEE Sensors Letters*, vol. 3, no. 6, pp. 1–4, Jun. 2019, doi: 10.1109/LSENS.2019.2916636.

[25] A. S. Edun, N. K. T. Jayakumar, S. Kingston, C. Furse, M. Scarpulla, and J. B. Harley, "Spread Spectrum Time Domain Reflectometry with Lumped Elements on Asymmetric Transmission Lines," *IEEE Sensors Journal*, pp. 1–1, 2020, doi: 10.1109/JSEN.2020.2967894.

[26] "ENF Ltd." /pv/panel-datasheet/crystalline/35078 (accessed Jan. 11, 2021).

[27] "Live Cable Fault Detection by LiveWire Innovation," *LiveWire Innovation*. https://www.livewireinnovation.com/ (accessed Jul. 06, 2020).

[28] "SENTINEL 100 SSTDR ENGINE," *LiveWire Innovation*. https://www.livewireinnovation.com/products/sstdr-engine/ (accessed Jul. 06, 2020).

[29] E. Benoit *et al.*, "Quantifying the Window of Uncertainty for SSTDR Measurements of a Photovoltaic System," *IEEE Sensors Journal*, vol. 21, no. 8, pp. 9890–9899, Apr. 2021, doi: 10.1109/JSEN.2021.3059412.